ACS Catalysis

Research Article

pubs.acs.org/acscatalysis

Preparation of Highly Dispersed Chromium Oxide Catalysts Supported on Mesoporous Silica for the Oxidative Dehydrogenation of Propane Using CO_2: Insight into the Nature of Catalytically Active Chromium Sites

Jayeon Baek, Hyeong Jin Yun, Danim Yun, Youngbo Choi, and Jongheop Yi*

World Class University Program of Chemical Convergence for Energy & Environment, Institute of Chemical Processes, School of Chemical and Biological Engineering, Seoul National University, Seoul 151-741, Republic of Korea

Supporting Information

ABSTRACT: Highly dispersed chromium oxide catalysts supported on mesoporous silica (Cr-MSU-*x*) were prepared via a $(N^0M^{n+})I^0$ pathway with the goal of achieving the high performance oxidative dehydrogenation of propane (ODHP) reaction. The resulting materials exhibited a mesopore structure resembling 3D wormhole-like holes, as characterized by N_2 adsorption−desorption isotherms and HR-TEM. Catalytic experimental results revealed that the catalyst with a 0.028 Cr/Si molar ratio showed the highest catalytic activity among the catalysts studied. Two types of chromium species, isolated Cr(VI) and polymeric Cr(VI) species, were observed, as evidenced by H_2-temperature-programmed reduction. They were designated as "hard Cr(VI)" and "soft Cr(VI)" sites, respectively. The initial composition of the soft Cr(VI) in the total Cr(VI) is a major determinant factor in the ODHP performance.

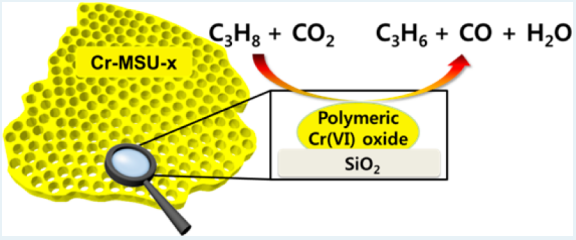

KEYWORDS: *Cr-MSU-x, oxidative dehydrogenation of propane, CO_2 utilization, active sites in chromium oxide*

1. INTRODUCTION

Propylene is one of the most important building blocks in the petrochemical industry for producing polypropylene, propylene oxide, and acrylonitrile.[1−3] The oxidative dehydrogenation of propane (ODHP) reaction is considered an attractive process alternative to steam cracking and FCC[1] for producing propylene. The ODHP reaction represents a route for economically converting low-cost saturated hydrocarbons into value-added olefins.[4−7] The use of oxygen as the oxidant in the ODHP reaction is thermodynamically favorable (an exothermic reaction) but shows low selectivity for propylene due to the fact that oxygen reacts readily with the products.[8−11] Carbon dioxide (CO_2) can be a substitute for oxygen, since it serves as a soft oxidant, thus preventing the overoxidation of the products.[12−14] In addition, reducing the levels of CO_2 and utilizing it are an urgent subject for realizing a sustainable society.[15−17]

A number of transition metal oxide catalysts, such as indium oxide, gallium oxide, vanadium oxide, and chromium oxide, have been reported to be active for the ODHP reaction.[2,18−23] In particular, chromium oxide has been shown to be highly active for the ODHP reaction in the presence of CO_2.[5,21] The low surface area of bulk crystalline chromium oxides, however, limits its use in this reaction. With the goal of preparing a catalyst with an abundance of active sites, we prepared a series of samples that contain highly dispersed chromium oxide on mesoporous silica with different amounts of chromium by a facile sol−gel method.

It is generally considered that coordinatively unsaturated Cr(III) in chromium species act as active sites in dehydrogenation reactions.[24−26] Accordingly, several groups have reported that coordinatively unsaturated Cr(III), formed from the reduction of higher-valence states (i.e. Cr(VI)), is an active site in this reaction.[27−30] This claim is supported by the fact that higher-valence chromium states are instantly reduced when they come into contact with alkanes at high temperature.[31]

Interestingly, the degree of crystallization of the chromium species is also considered to be another important factor in the dehydrogenation reaction. Kumar et al.[31] reported that isolated chromium species are more active for the dehydrogenation reaction than crystalline α-Cr_2O_3 when SBA-15 is used as the support, whereas oligomeric chromium species are more active than isolated chromium species when γ-Al_2O_3 is used as the support. However, they were not able to compare the catalytic activity of chromium species (isolated vs oligomers) on SBA-15 because oligomeric chromium species supported on SBA-15 were not prepared. Consequently, this implies that the synthesis of the polymeric Cr(VI) species on mesoporous silica results in an efficient catalysts for the ODHP reaction and could function as an active center.

MSU-*x* family, a typical mesoporous silica, has uniform and three-dimensional wormhole-like channels[32] which is favorable

Received: March 23, 2012
Revised: July 19, 2012
Published: July 20, 2012

for the diffusion of molecules as well as a high surface area and, thus, could be utilized as a promising catalyst support.[24] Here, *x* is a number or a letter of the used surfactant type. To date, chromium-based mesoporous silica catalysts have been synthesized under highly acidic (Cr-SBA-1,[33] Cr-SBA-15,[34] and Cr-MSU-*x*[28]) or basic (Cr-MCM-41[35]) conditions. The types of chromium species formed are, however, strongly dependent on the pH of the aqueous solution used in the synthesis.[36] At pH values lower than 2, chromium species are formed as tri- and tetrachromates (respectively, $Cr_3O_{10}^{2-}$ and $Cr_4O_{13}^{2-}$) which are more highly polymerized and susceptible to forming crystalline α-Cr_2O_3. In the pH range of 2−6, smaller chromium anions, such as dichromate ($Cr_2O_7^{2-}$), are formed., which leads to a better dispersion of chromium species on the MSU-*x* surface.

Above pH 8, only isolated CrO_4^- is stable, but it does not possess a high activity for the ODHP reaction. Therefore, we developed a new method for the synthesis of highly dispersed chromium oxide on a MSU-*x* support at pH ∼ 4 without any additional titration for use as a potentially promising catalyst for ODHP reactions using chromium(III) acetate hydroxide ($((CH_3CO_2)_7Cr_3(OH)_2)$). Here, we used a $(N^0M^{n+})I^0$ pathway developed by Pinnavaia et al.[37] wherein N^0 is a nonionic polyethylene oxide surfactant and I^0 is an electrically neutral silica precursor. An electrostatic control is introduced into the assembly process through chromium cations (M^{n+}). Our strategy involved the use of chromium(III) acetate hydroxide ($((CH_3CO_2)_7Cr_3(OH)_2)$), which provides the electrostatic driving force for the ($(N^0M^{n+})I^0$, M^{n+}: Cr^{3+}) pathway and also functions as a precursor for active materials. The steric effect of the ligand in ($((CH_3CO_2)_7Cr_3(OH)_2)$) also helps the chromium species to be highly dispersed on the catalyst support, similar to chromium acetyl acetonate ($Cr(acac)_3$).[27]

In the present work, highly dispersed chromium oxide on MSU-*x* (Cr-MSU-*x*) with different amounts of chromium was prepared with the goal of creating chromium species in which the activity is dependent on the weight of metal loading.[38,39] This would enable one to investigate the nature of the chromium species and the catalytic function of each specific chromium state in the ODHP reaction. The correlation between catalytic activity and characterization results obtained from temperature-programmed reduction experiments would permit a better understanding of the nature of the active chromium species for ODHP reaction. We then compared the Cr-MSU-*x* catalysts with the CrO_x/MSU-*x* catalysts prepared using the conventional incipient wetness impregnation method.

2. EXPERIMENTAL SECTION

2.1. Preparation of the Cr-MSU-*x*N Catalysts. Polyethylene glycol hexadecyl ether (Brij c10), chromium(III) acetate hydroxide ($((CH_3CO_2)_7Cr_3(OH)_2)$), and tetraethyl orthosilicate (TEOS) were purchased from Sigma-Aldrich and were used as the sources of template, chromium, and silicon, respectively. A typical procedure for preparing Cr-MSU-*x* catalysts is described as follows: A solution of surfactant was prepared by resolving 1.78 g of Brij c10 in 100 mL of water at 45 °C under rigorous stirring. A weighed amount of the chromium precursor ($((CH_3CO_2)_7Cr_3(OH)_2)$) was then dissolved in the surfactant solution, where the Cr/Brij c10 molar ratio ranged from 0.1 to 2.5. The solution of surfactant and chromium was then stirred at 45 °C overnight to completely dissolve the acetate form of chromium. After adding 14.5 mL of TEOS to the mixed solution of surfactant and chromium, the resulting solution was stirred at 45 °C for 24 h. The color of the resulting solutions was initially a pale green but became dark green with increasing molar ratio of Cr/Brij c10. The resulting solutions were then placed in an oven and aged without stirring at 100 °C for 24 h. The solid products were separated by filtration, washed thoroughly with deionized water, and dried at room temperature for 48 h. The final products were obtained after calcination in a stream of air at 650 °C for 3 h to remove the template. Here, we denote the Cr-MSU-*x*N where *N* indicates the Cr/Si molar ratio multiplied by 10^3.

2.2. Preparation of Reference Materials. A pure MSU-*x* catalyst was prepared according to a previously reported method.[37] Instead of ($((CH_3CO_2)_7Cr_3(OH)_2)$), cobalt(II) chloride hexahydrate ($CoCl_2{\cdot}6H_2O$) was used as a metal cation in the $(N^0M^{n+})I^0$ pathway. After calcination of the resulting products, no elemental cobalt was present, as evidenced by SEM-EDS analysis. CrO_x/MSU-*x* was prepared by the incipient wetness impregnation method using $Cr(NO_3)_3{\cdot}9H_2O$, where the Cr/Si molar ratio was equal to that for the highest performance among the Cr-MSU-*x* catalysts series.

2.3. Characterization. Elemental analyses of the Cr-MSU-*x* catalysts series were performed by scanning electron microscopy (SEM, Zeiss Supra 55) equipped with an energy-dispersive X-ray spectroscopy (EDS) module with an accelerating voltage of 15 kV. The X-ray diffraction (XRD) patterns were obtained in two ranges of 1−10° and 10−80° using a SAXS with GADDS and Rigaku D-MAX2500-PC powder X-ray diffractometer, respectively, with Cu Kα radiation (1.5406 Å). The N_2 adsorption−desorption isotherms were recorded on a Micrometrics ASAP-2010 system.

The specific surface area of the samples was determined by the BET method. The total pore volume and pore size distributions were calculated from the adsorption branches of the isotherms using BJH methods. High-resolution transmission electron micrograph (HR-TEM) images were obtained on a JEOL JEM-3010 microscope with an acceleration voltage of 300 kV.

To explore the element distribution mapping on the samples, an analytical high-angle annular dark-field scanning transmission electron microscope (HAADF-STEM, Tecnai F20-FEI, 200 kV) equipped with energy dispersive X-ray spectroscopy (EDS, Tecnai 136−5-EDAX) was used. ^{29}Si MAS NMR spectra of the samples were recorded on a Bruker Avance II 500 MHz spectrometer operating at a frequency of 99.4 MHz. The magic angle spin speed used for ^{29}Si spectral recording was 7 kHz.

Ultraviolet−visible (UV−vis) spectra were recorded with a Jasco V670 spectrometer, using diffuse reflectance spectroscopy (DRS) technique. The powdery sample was loaded into a quartz cell, and spectra were collected at 200−1000 nm referenced to $BaSO_4$. UV-Raman spectroscopic measurements were carried out on a MonoRa750i/ELT1000 spectrometer. The spectra were recorded with a 325 nm excitation laser provided by a He−Cd source. Spectra were recorded at an exposure time of 30s and an accumulation number of 5.

Fourier transform infrared attenuated total reflection (FT-IR/ATR) spectra were obtained using a PerkinElmer Spectrum 100 FT-IR. A diamond prism was used as an internal reflecting element for the FT-IR/ATR analysis. The temperature-programmed reduction analysis was performed with a Micrometrics Autochem II chemisorption analyzer using a 10% H_2/Ar mixture at a total flow rate 50 cm^3 min^{-1}. The sample was heated at a rate of 10 °C min^{-1} to the final temperature of 600 °C. H_2 consumption during the TPR experiments was

dx.doi.org/10.1021/cs300198u | ACS Catal. 2012, 2, 1893−1903

Table 1. Physicochemical Properties of the Pure MSU-*x* and Cr-MSU-*x*N Catalysts

catalyst[a]	Cr (wt %)	Si (wt %)	Cr/Si molar ratio	surface area ($m^2 \cdot g^{-1}$)	av pore size (nm)	pore volume ($cm^3 \cdot g^{-1}$)
pure MSU-*x*				876	4.8	1.06
Cr-MSU-*x*3	0.18	26.07	0.003	903	4.5	1.03
Cr-MSU-*x*10	0.46	26.67	0.010	896	4.1	0.93
Cr-MSU-*x*14	0.62	22.80	0.014	848	4.2	0.90
Cr-MSU-*x*28	1.27	24.44	0.028	791	4.5	0.88
Cr-MSU-*x*51	2.16	22.98	0.051	754	4.2	0.78
Cr-MSU-*x*82	3.59	23.79	0.082	730	3.9	0.71

[a]Cr-MSU-*x*N, where *N* indicates the Cr/Si molar ratio multiplied by 10^3.

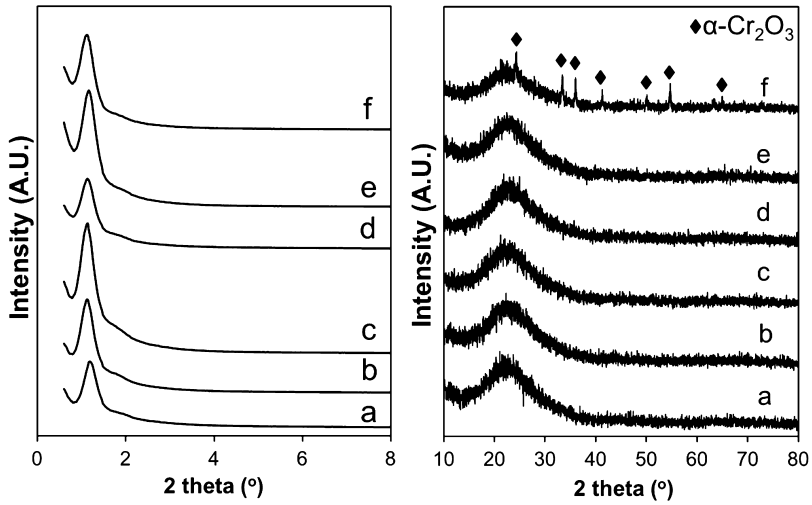

Figure 1. XRD powder patterns of Cr-MSU-*x*N catalysts: (a) Cr-MSU-*x*3, (b) Cr-MSU-*x*10, (c) Cr-MSU-*x*14, (d) Cr-MSU-*x*28, (e) Cr-MSU-*x*51, and (f) Cr-MSU-*x*82.

measured by means of a thermal conductivity detector (TCD). The amount of coke deposited on the catalyst was determined by CHNS analysis (CHNS-932, LECO). The over-reduction of the catalyst was carried out in a stream of 10% H_2/Ar gas (50 $cm^3 min^{-1}$) at 650 °C for 3 h using a Micrometrics Autochem II chemisorption analyzer.

2.4. Catalytic Reactions. The dehydrogenation of propane in the presence of CO_2 was carried out in a flow-type quartz reactor packed with 200 mg of catalyst, and the reactor was then placed in an electric furnace. The temperature of the catalyst bed was monitored by a K-type thermocouple controlled by a PID controller. The catalyst was preheated at 600 °C in a stream of dry N_2 (30 cm^3 min^{-1}) for 0.5 h. The dehydrogenation feed consisted of a mixture of $C_3H_8/CO_2/N_2$ = 1:1:8, and the total flow rate was 30 cm^3 min^{-1}. For the controlled experiment, direct dehydrogenation of propane in the absence of CO_2 was carried out using C_3H_8/N_2 = 1:9 feed. The feed and reaction products were analyzed using an online gas chromatograph (Donam DS 6200) equipped with two columns (Porapak Q and molecular sieve) and two detectors (flame ionization detector and thermal conductivity detector). CO_2 and C2−C3 hydrocarbons were separated in a column packed with the Porapak Q, whereas N_2, CO, and C1 were separated using a molecular sieve. FID and TCD were used for quantification of C1−C3 hydrocarbons and nonhydrocarbons (N_2, CO, and CO_2), respectively. The regeneration treatment was carried out under a stream of air (50 mL/min) at 650 °C for 3 h, followed by an ODHP reaction test. The conversion, selectivity, and yield of propylene were calculated using the following equations:

$$C_3H_8 \text{ conversion } (\%) = \frac{C_3H_{8in} - C_3H_{8out}}{C_3H_{8in}} \times 100$$

$$C_3H_6 \text{ selectivity } (\%) = \frac{nC_3H_6}{nC_3H_6 + (2/3)nC_2H_6 + (2/3)nC_2H_4 + (1/3)nCH_4} \times 100$$

$$C_3H_6 \text{ yield } (\%) = \frac{C_3H_8 \text{ conversion} \times C_3H_6 \text{ selectivity}}{100}$$

where *n* is a number of moles of hydrocarbons. Because the coke formation is instantaneous and time-dependent, the conversion of propane into coke was not considered in the calculations. In addition, the conversion of propane to coke, as measured by CHNS, for the catalyst after a 2 h ODHP reaction was 1.1 wt %.

3. RESULTS AND DISCUSSION

3.1. Highly Dispersed Chromium Oxide Catalysts Supported on MSU-*x* Materials with Mesoporous Structure. The Cr and Si elemental contents of the Cr-MSU-*x*N catalysts are summarized in Table 1. As the amount of chromium precursor used in the synthesis process was increased, the Cr/Si molar ratio also increased from 0.003 to 0.082. Figure 1 shows XRD patterns of the Cr-MSU-*x*N catalysts in two different regions of 2θ angles. In the 2θ range of 1−10°, a single broad diffraction line is observed at about 2θ = 1.08°, corresponding to d_{100} (8.2 nm) reflections and in agreement with most patterns of MSU-*x* materials reported by

dx.doi.org/10.1021/cs300198u | ACS Catal. 2012, 2, 1893−1903

other investigators.[28,32] Even in the case of the catalyst with the highest chromium loading (Cr-MSU-*x*82), a single peak at 2θ = 1.08° is still observed, indicating that the mesoporous structure of the materials was maintained. In the 2θ range of 10−80°, only the characteristic peak related to silica is observed up to a Cr/Si molar ratio of 0.051. This means that chromium oxide is highly dispersed on MSU-*x*, and as a result, its size is too small to be detectable. On the other hand, the Cr-MSU-*x*82 catalyst shows peaks related to crystalline chromium oxide, indicating the formation of α-Cr_2O_3.

The N_2 adsorption−desorption isotherm and pore size distribution of the pure MSU-*x* and Cr-MSU-*x*51 (the largest amount of chromium among the samples without any formations of crystalline chromium oxide) are shown in Figure 2. The isotherms of the pure MSU-*x* and the Cr-MSU-*x*51

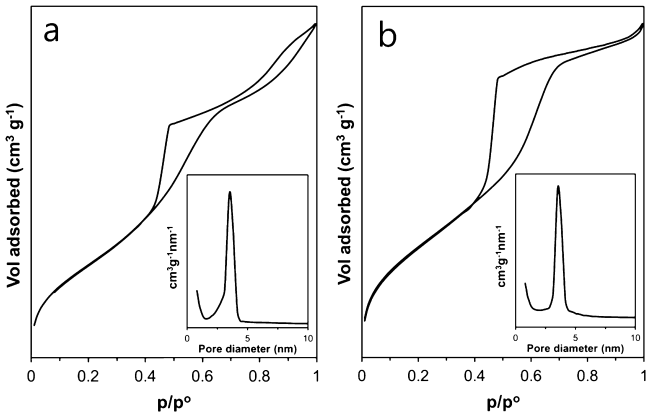

Figure 2. N_2 adsorption−desorption isotherms and pore size distributions of (a) pure MSU-*x* and (b) Cr-MSU-*x*51 materials.

catalyst are similar to a type IV isotherm and exhibit a H2 type hysteresis loop at relative pressures ranging from 0.4−0.7, except for the fact that the pure MSU-*x* contains additional textural pores. This indicates that both pure MSU-*x* and Cr-MSU-*x*51 catalyst have well-developed mesoporous structures with pore necking in the 3D faulted structure.[37] The pore size, calculated from the BJH adsorption branch, is in the range from 2 to 5 nm for both the pure MSU-*x* and Cr-MSU-*x*51 catalysts, and their average pore size is about 4.8 and 4.2 nm, respectively. In addition, all the other Cr-MSU-*x*N catalysts show similar isotherms and pore size distributions (see Supporting Information Figure S1) indicating that the overall mesoporous structure is well maintained, even when a high amount of chromium is deposited on the MSU-*x* surface. The surface area and pore volume of the Cr-MSU-*x*N catalyst series do, however, decrease with an increase in the Cr/Si molar ratio, indicating that mesopores in Cr-MSU-*x*N are covered by chromium oxide when relatively high amounts of chromium are used in the preparation (Table 1).

The HR-TEM image (Figure 3a) confirms that the Cr-MSU-*x*51 catalyst contains three-dimensional wormhole-like channels. The pore size, as determined from TEM images, is in good agreement with the average pore size from BJH result. TEM images for the other Cr-MSU-*x* catalysts are shown in Supporting Information Figure S2. To examine the dispersion of chromium oxide, an analytical STEM with large angle detection was used for 2-D atomic mapping (Figure 3b and c). From this 2-D atomic mapping image, we were able to confirm that small clusters of chromium oxide are highly dispersed throughout an entire Cr-MSU-*x*51 structure without the formation of a large bulk state of chromium oxide. This highly dispersed chromium is also consistent with data for Cr-MSU-*x*28 (see Supporting Information Figure S3).

^{29}Si MAS NMR spectra of pure MSU-*x* and Cr-MSU-*x*28 are shown in Figure 4. There are three distinct peaks

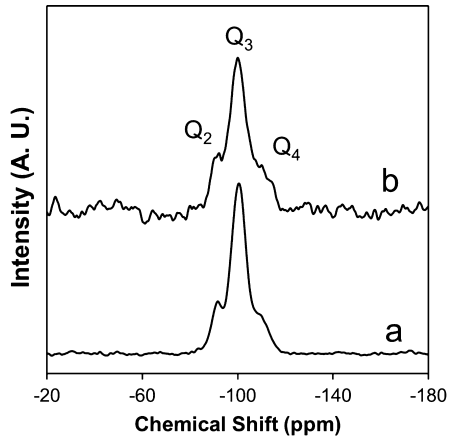

Figure 4. ^{29}Si MAS NMR spectra of the (a) pure MSU-*x* and (b) Cr-MSU-*x*28 materials.

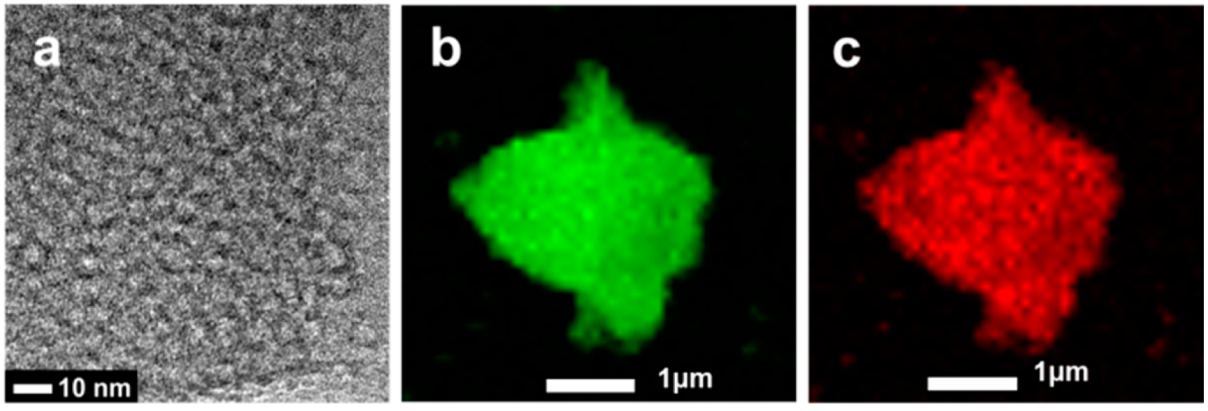

Figure 3. Morphological and compositional studies of Cr-MSU-*x*51 catalyst obtained by microscopy techniques. (a) HR-TEM image of Cr-MSU-51 and 2-D atomic mapping by using analytical STEM equipped with EDS; (b) Si and (c) Cr.

dx.doi.org/10.1021/cs300198u | *ACS Catal.* 2012, 2, 1893−1903

corresponding to Q^2, Q^3, and Q^4 in both the pure MSU-x and Cr-MSU-x28 materials with no noticeable differences between the two. According to Pinnavaia et al.,[40] broadening of the Q^4 peak width and the decrease in Q^2 and Q^3 Si sites along with an increase in Q^4 are mainly caused by substitution with an isomorphous transition metal substitution. Maintaining three sites of silica indicates that isomorphous chromium metal substitution did not occur after the chromium precursor was added.

3.2. Characterization of the Chromium Species. The oxidation state and coordination of chromium in Cr-MSU-xN catalysts can critically influence catalytic activity. To investigate this, UV−vis DRS experiments were carried out. All spectra of the Cr-MSU-xN catalysts are given in Figure 5. Two intense

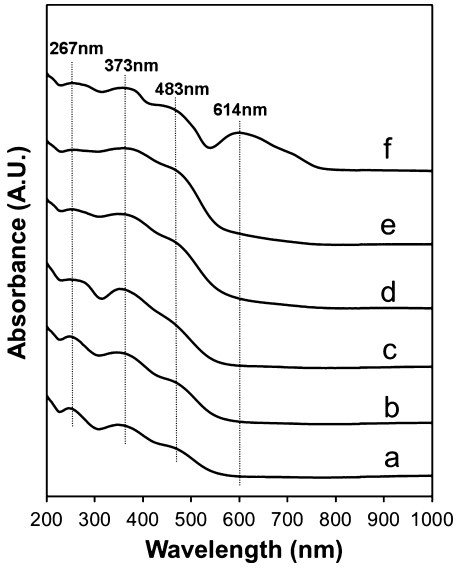

Figure 5. Diffuse reflectance UV−vis spectra of Cr-MSU-xN catalysts: (a) Cr-MSU-x3, (b) Cr-MSU-x10, (c) Cr-MSU-x14, (d) Cr-MSU-x28, (e) Cr-MSU-x51, and (f) Cr-MSU-x82.

bands centered at 267 and 373 nm, which are usually assigned to O → Cr(VI) charge transfers in isolated chromium oxide with a tetrahedral symmetry, appeared as the main absorption bands for all samples listed in Figure 4.[28] These two bands at 267 and 373 nm are assigned to tetrahedral chromate transitions $^1T_2 \leftarrow {}^1A_1$ ($1t_1 \rightarrow 7t_2$ and $6t_2 \rightarrow 2e$) and $^1T_2 \leftarrow {}^1A_1$ ($1t_1 \rightarrow 2e$), respectively. The peak at 483 nm is also assigned to a Cr(VI) transition $^1T_1 \leftarrow {}^1A_1$ ($1t_1 \rightarrow 2e$).[41] The intensity of this peak increases gradually as the Cr/Si molar ratio is increased up to 0.051. This band is closely related to the distortion of the Cr(VI) group from a tetrahedral symmetry.

The distortion of isolated chromium oxide is reported by Cavani et al.[41] to be related to the degree of oligomerization in the chromium species, that is, the formation of dimers or polymeric chromium oxide as a consequence of polymerization process. Therefore, the gradual increase in the intensity at 483 nm is caused by the formation of oligomers, which have a lower symmetry than a tetrahedral structure. When the Cr/Si molar ratio increases to 0.082, a new band at 614 nm appears while the band at 483 nm is slightly decreased. The band at 614 nm corresponds to the typical octahedral symmetry $T_{2g} \leftarrow A_{2g}$ transition in α-Cr_2O_3 clusters.[34,42] Thus, the appearance of the peak at 614 nm and the decrease in the intensity of the band at 483 nm is caused by the formation of crystalline chromium oxide. These UV−vis DRS results are consistent with data obtained in the XRD experiments.

UV-Raman spectra of Cr-MSU-xN catalysts are shown in Figure 6. Here, UV-Raman spectroscopy was used to avoid the

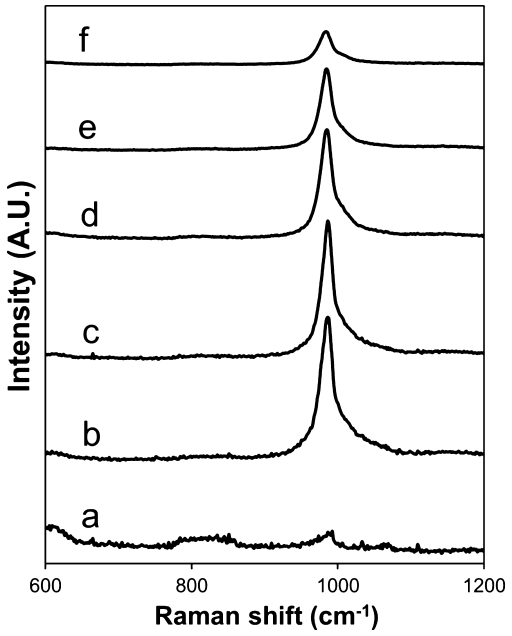

Figure 6. UV-Raman spectra of Cr-MSU-xN catalysts: (a) Cr-MSU-x3, (b) Cr-MSU-x10, (c) Cr-MSU-x14, (d) Cr-MSU-x28, (e) Cr-MSU-x51, and (f) Cr-MSU-x82.

fluorescence interference from the molecular sieves or related materials.[43] In the presented data, an intense and sharp band at 983 cm^{-1} is observed in the case of the Cr-MSU-xN catalysts, whereas the band intensity is very low in the Cr-MSU-x3 sample. Wechhuysen et al.[36] reviewed the Raman spectra of a number of supported chromium oxides and concluded that the band at 980−990 cm^{-1} can be assigned to Cr−O stretching of the dehydrated isolated chromate species (CrO_4^{2-}), and the band at 1000−1010 cm^{-1} can be ascribed to the Cr−O stretching of dehydrated polymeric chromium oxide. Unfortunately, overlapping of two bands made it difficult to discriminate polymeric chromium oxide from isolated chromium oxide. As the chromium concentration increases, the band at 983 cm^{-1} decreases, indicating that polymeric chromium species are formed during the polymerization process of isolated chromium oxides.

FT-IR spectroscopy is a useful technique for characterizing chromium species in catalysts. Figure 7 shows the FT-IR/ATR results for the Cr-MSU-xN catalysts. The high-frequency region between 1000 and 1250 cm^{-1} corresponds to silicon−oxygen stretching motions, and the band at 796 cm^{-1} is assigned to the vibration of silicon about bridged oxygen.[44] A weak IR band appears at 900 cm^{-1}, a much lower value than has been previously assigned in other literature reports to a Cr(VI)-O vibration at about 941 and 950 cm^{-1} in the Cr-SBA-15 and CrO_x/SBA-15 samples, respectively.[34] This shift might be caused by differences in the local environments in Cr-MSU-xN catalysts, Cr-SBA-15, and CrO_x/SBA-15. Meanwhile, the Cr(VI)-O vibration band increases gradually up to a Cr/Si molar ratio of 0.051, indicating an increase in the polymeric Cr(VI) concentration. In the case of the Cr-MSU-x82 spectrum, the 900 cm^{-1} band has nearly disappeared, while

dx.doi.org/10.1021/cs300198u | ACS Catal. 2012, 2, 1893−1903

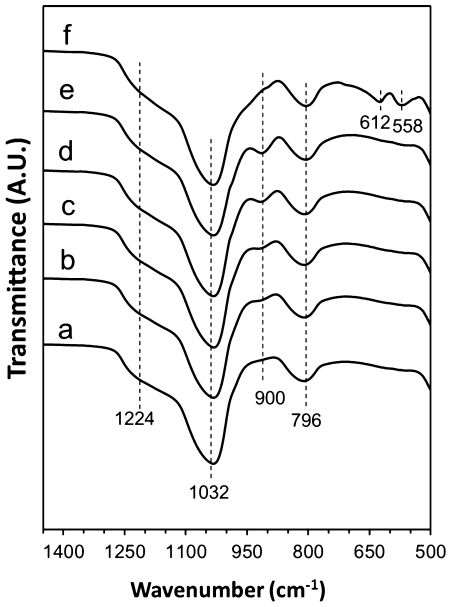

Figure 7. FT-IR/ATR spectra of Cr-MSU-*x*N catalysts: (a) Cr-MSU-*x*3, (b) Cr-MSU-*x*10, (c) Cr-MSU-*x*14, (d) Cr-MSU-*x*28, (e) Cr-MSU-*x*51, and (f) Cr-MSU-*x*82.

two distinct bands are observed at 558 and 612 cm^{-1} which are characteristic of crystalline α-Cr_2O_3.[45]

3.3. Reducibility of the Cr-MSU-*x*N Catalysts. The reducibility of a catalyst plays a key role in dehydrogenation reactions that involve a redox mechanism:

$$C_3H_8 + MeO_x \rightleftharpoons C_3H_6 + MeO_{x-1} + H_2O \quad (1)$$

$$CO_2 + MeO_{x-1} \rightleftharpoons CO + MeO_x \quad (2)$$

Therefore, the ability to remove hydrogen from propane is related to the reduction of the chromium species in Cr-MSU-*x*. H_2-TPR profiles of the Cr-MSU-*x*N catalysts are shown in Figure 8. The presented peaks are normalized by the weight percent of chromium in the Cr-MSU-*x*N catalysts. The

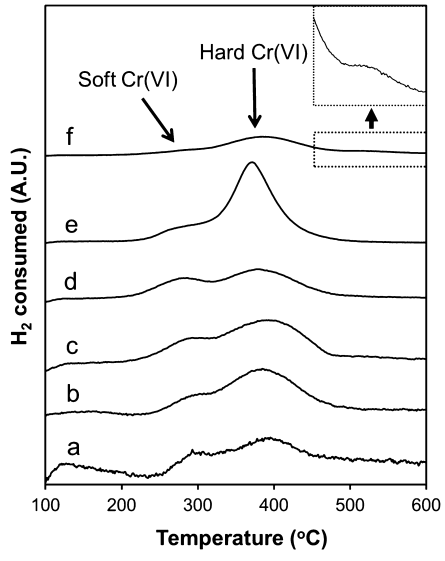

Figure 8. H_2-TPR profiles of Cr-MSU-*x*N catalysts: (a) Cr-MSU-*x*3, (b) Cr-MSU-*x*10, (c) Cr-MSU-*x*14, (d) Cr-MSU-*x*28, (e) Cr-MSU-*x*51, and (f) Cr-MSU-*x*82.

appearance of reduction peaks can be affected by either the amount of chromium or the interaction between chromium oxide and the support. Two reduction peaks at about 270 and 380 °C can be seen for all samples, and this can be attributed to the reduction of Cr(VI) to Cr(III) and Cr(II), as well.[24,28,46,47] The TPR results combined with the UV−vis DRS results above clearly show that chromium exists as the Cr(VI) state in the samples prepared using Cr/Si molar ratios ranging from 0.003 to 0.051. The observation of two reduction peaks, supposedly originating from the reduction of Cr(VI) species in and out of the framework, has been reported elsewhere.[28]

In-situ Raman spectroscopy studies performed by Weckhuysen et al.[48] have confirmed two types of surface chromium oxide species on the inorganic oxide: an isolated species, which is difficult to reduce, and a polymeric species, which is more easily reduced on the same support. Therefore, the lower and the higher reduction peaks are assumed to be polymeric Cr(VI) oxide and isolated Cr(VI) oxide, respectively. This is explained by the weaker interaction of the polymeric chromium oxide with the support, which causes the material to be soluble in water.[27,30,41] UV−vis DRS and FT-IR/ATR results that provide confirmation of a polymerization process also support this conclusion. Here, we use the term "soft Cr(VI)" and "hard Cr(VI)" to refer to Cr(VI) oxide that are easy and difficult to reduce, respectively. Cr-MSU-*x*82 shows another reduction peak at over 500 °C that is assigned to α-Cr_2O_3.

Zhang et al. reported on the reduction of α-Cr_2O_3 at a higher temperature than the isolated or polymeric chromium oxide.[34] H_2 consumption per gram of catalyst and the ratio of H_2/Cr are presented in Table 2. The amount of consumed H_2 increases until the Cr/Si molar ratio reaches 0.051 and decreases in Cr-MSU-*x*82 sample. This is because α-Cr_2O_3 is dominant in the Cr-MSU-*x*82 sample.

The ratio of H_2/Cr allows one to estimate the amount of redox Cr(VI) species in the fresh Cr-MSU-*x*N catalysts. The area for soft and hard Cr(VI) were calculated from the deconvoluted Gaussian lines from the normalized reduction peaks, as seen in Table 2. The area of the soft Cr(VI) reaches a maximum up to Cr-MSU-*x*14 and Cr-MSU-*x*28 catalysts and then decreases. The hard Cr(VI) area is largely increased as the Cr/Si molar ratio increases to 0.01 and decreases slightly until the Cr/Si molar ratio reaches 0.028 and drastically increases again at a Cr/Si molar ratio of 0.051. The ratio of soft Cr(VI) to total Cr(VI) is the highest for the Cr-MSU-*x*28 catalyst. This indicates that the Cr-MSU-*x*28 catalyst contains mainly polymeric Cr(VI) oxides together with isolated Cr(VI) oxide as a minor phase, and the soft Cr(VI) might undergo redox processes quite effectively.

3.4. Catalytic Performance. Figure 9 shows time on-stream catalytic activity with respect to catalytic reaction temperature: 400, 500, 600, and 700 °C. The catalytic activity increases linearly with increasing temperature. Selectivity, however, drops dramatically at a reaction temperature of 700 °C. The use of CO_2 in the dehydrogenation of propane instead of O_2 is to enhance the selectivity of the reaction for propylene as referred to above. Thus, both a high activity and acceptable selectivity are achieved at 600 °C, and this is considered to be the most suitable reaction temperature. The catalytic performance of the Cr-MSU-*x*N catalysts for the dehydrogenation of propane using CO_2 was therefore examined at 600 °C. In a blank experiment without catalyst at 600 °C, propane conversion was 20%, and the selectivity for propylene was 50%, which corresponds to a 10% yield.

dx.doi.org/10.1021/cs300198u | ACS Catal. 2012, 2, 1893−1903

Table 2. Reducibility of the Cr-MSU-*x*N Catalysts from H_2-TPR Profiles

catalyst[a]	H_2 consumption (mmol·g^{-1})	H_2/Cr	soft Cr(VI) area[b]	hard Cr(VI) area[b]	soft/total Cr(VI) area
Cr-MSU-*x*3	0.046	1.33	0.08	0.84	0.089
Cr-MSU-*x*10	0.14	1.55	0.15	1.16	0.12
Cr-MSU-*x*14	0.21	1.73	0.35	1.08	0.25
Cr-MSU-*x*28	0.30	1.21	0.32	0.72	0.30
Cr-MSU-*x*51	0.76	1.83	0.22	1.27	0.15
Cr-MSU-*x*82	0.46	0.67	0.06	0.46	0.12

[a]Cr-MSU-*x*N, where *N* indicates the Cr/Si molar ratio multiplied by 10^3. [b]Soft and hard Cr(VI) area was calculated from the deconvoluted Gaussian lines from the normalized reduction peaks (Figure 8)

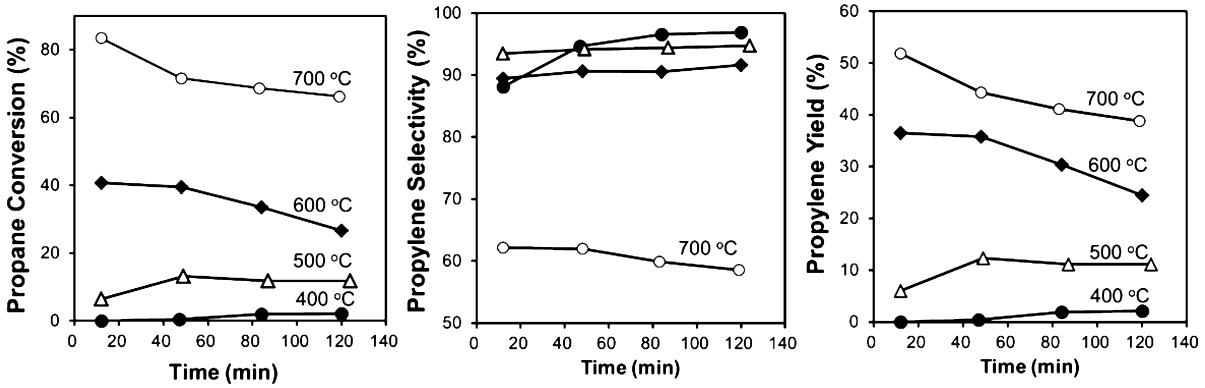

Figure 9. Time on-stream for propane conversion, selectivity, and propylene yield over Cr-MSU-*x*28 catalyst at various ODHP reaction temperatures: (●) 400 °C, (Δ) 500 °C, (♦) 600 °C, and (○) 700 °C.

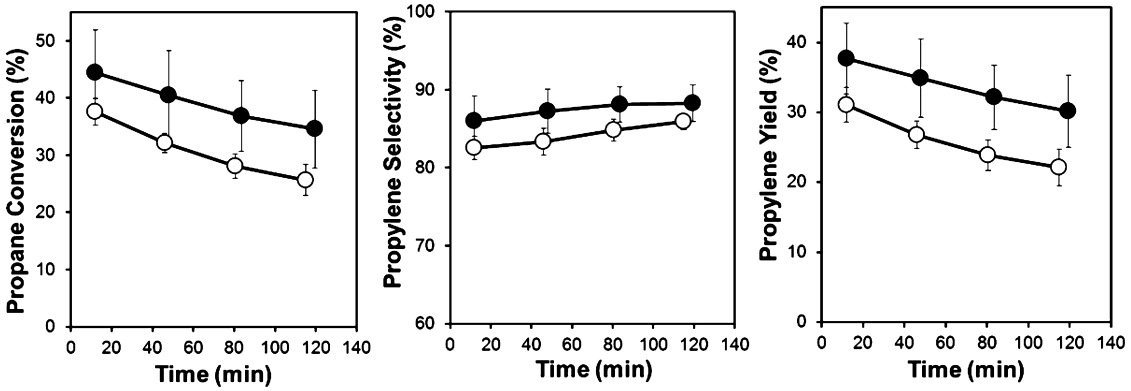

Figure 10. Time on-stream for propane conversion, selectivity, and propylene yield over Cr-MSU-*x*28 catalysts: (●) oxidative dehydrogenation of propane using CO_2 and (○) direct dehydrogenation of propane without CO_2.

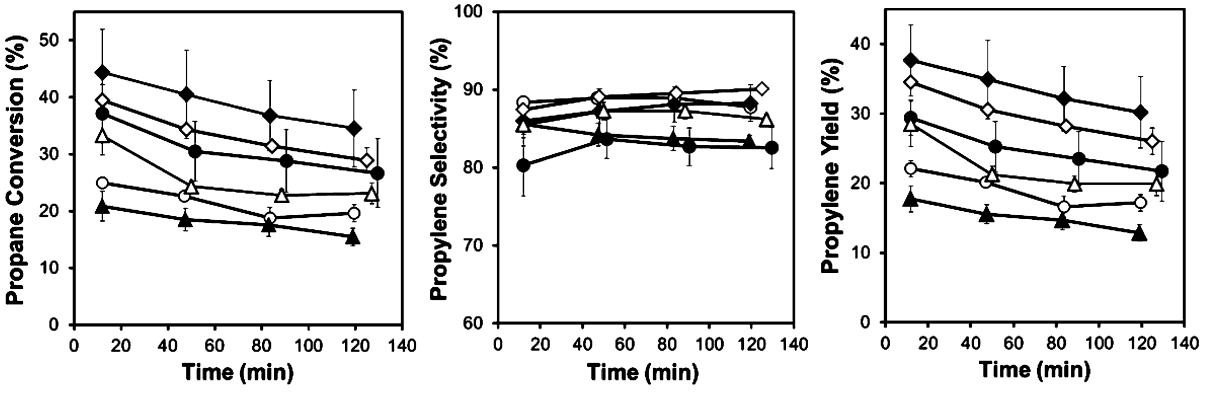

Figure 11. Time on-stream for propane conversion, selectivity, and propylene yield over Cr-MSU-*x*N catalysts: (▲) Cr-MSU-*x*3, (○) Cr-MSU-*x*10, (●) Cr-MSU-*x*14, (♦) Cr-MSU-*x*28, (◊) Cr-MSU-*x*51, and (Δ) Cr-MSU-*x*82.

dx.doi.org/10.1021/cs300198u | *ACS Catal.* 2012, 2, 1893−1903

To investigate the contribution of CO_2 in ODHP reaction, catalytic tests using C_3H_8/N_2 and $C_3H_8/CO_2/N_2$ feeds were compared. The results shown in Figure 10 clearly indicate that the presence of CO_2 markedly improved the yield of propylene. This catalytic performance can be evidence that CO_2 plays the promoting role in the conversion of propane to propylene over Cr-MSU-*x*N catalysts. This promoting effect can be rationalized as that CO_2 can play a role in the consumption of H_2 produced by the dehydrogenation of propane via a reverse water-gas shift reaction. The reaction can be given as follows:

$$C_3H_8 \rightleftharpoons C_3H_6 + H_2 \quad (3)$$

$$CO_2 + H_2 \rightleftharpoons CO + H_2O \quad (4)$$

The reduction of the partial pressure of hydrogen shifts the dehydrogenation equilibrium toward propylene and CO formation. From the GC data, the correlation between the CO area and propylene yield with respect to Cr/Si molar ratio was plotted in Supporting Information Figure S4. The CO area increases with an increase in the Cr/Si molar ratio up to 0.028 and then decreases slightly with further Cr/Si molar ratio, which has a similar correlation with catalytic activity. It can therefore be concluded that the CO_2 has a promotional effect in the ODHP reaction by participating in the RWGS reaction and that soft Cr(VI) is mainly responsible for this reaction.

Time-on-stream behavior for catalytic activity over the Cr-MSU-*x* catalyst series is shown in Figure 11. During the 2-h catalytic reaction, propane conversion and propylene yield decreased within 10%, and selectivity ranged between 80 and 90% with little change. Figure 12 shows the catalytic activity of

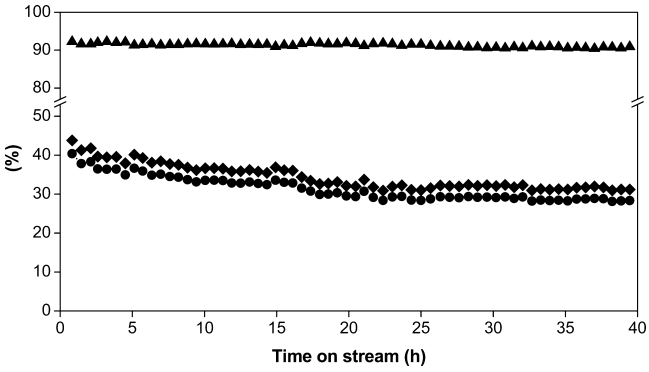

Figure 12. Propane conversion (♦), propylene selectivity (▲), and propylene yield (●) for Cr-MSU-*x*28 catalyst as a function of reaction time.

the Cr-MSU-*x*28 catalyst with time on-stream. Propane conversion drops with reaction time and approaches a steady state in 25 h, showing a 30% yield of propylene.

Deactivation was investigated in two ways: (i) coke formation and (ii) a reduction in active chromium sites. It has been reported that CO_2 acts as a soft oxidant that reduces the coke deposition by the reverse Boudouard reaction ($CO_2 + C \rightarrow 2CO$) and regenerates the reduced active Cr(III) sites.[1,12] Supporting Information Table S1 shows the amount of coke deposited on the catalyst before and after ODHP reaction over Cr-MSU-*x*28 catalyst. After 120 min over the ODHP reaction, 1.1 wt % of coke was deposited, which is not sufficiently significant to cause rapid deactivation.

To investigate the effect of the reduction of active chromium sites during the ODHP reaction on the catalyst deactivation, over-reduction was applied on Cr-MSU-*x*28 catalyst under a 10% of H_2/Ar gas stream (50 cm^3/min^{-1}) at 650 °C for 3 h. After the over-reduction of the Cr-MSU-*x*28 catalyst, the initial ODHP catalytic activity was decreased (Supporting Information Figure S5). This result strongly supports the conclusion that the main cause of initial catalytic deactivation is the reduction of active chromium sites. Even after the rapid deactivation, the catalytic activity was slowly decreased again. Shishido et al.[49] observed that the $Cr(VI)O_4$ tetrahedron was reduced to the $Cr(III)O_6$ octahedron and then converted to an aggregated form of the $Cr(III)O_6$ octahedron during the reaction using Cr K-edge XAFS spectroscopy. It appears that the aggregation of $Cr(III)O_6$ species can cause another decrease in the activity. The regenerative cycles of Cr-MSU-*x*28 catalyst are represented in Figure 13. The propylene yield

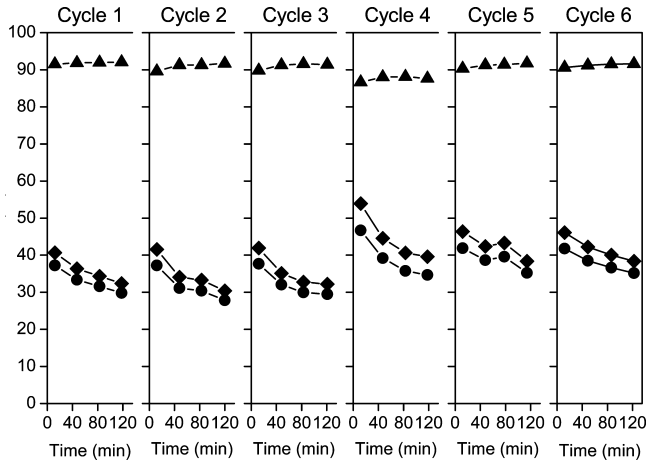

Figure 13. Regeneration treatment of the Cr-MSU-*x*28 catalyst with air at 650 °C for 3 h; propane conversion (♦), propylene selectivity (▲), and propylene yield (●).

on the catalyst decreases from 40% to 30% after 120 min on-stream in the first cycle. The regeneration step was carried out with an air stream at 650 °C for 3 h to reoxidize the reduced active chromium species. After the regeneration step, the propylene yield was 40%, which is the initial value, indicating that the original activity of the catalyst was fully recovered.

The relation between initial catalytic activity and Cr/Si molar ratio is shown in Figure 14. Propylene yields show a trend similar to that of propane conversion as a result of the nearly constant selectivity for propylene, regardless of the amount of chromium in the samples. The conversion of propane and the yield of propylene increases steeply with increasing amounts of chromium and reach a maximum at a Cr/Si molar ratio of 0.028. The existence of a maximum in catalytic performance indicates that an optimum Cr/Si molar ratio exists. Additional chromium results in a decrease in both the conversion of propane and the yield of propylene. This can be explained by formation of less active, crystalline α-Cr_2O_3, as confirmed by XRD, UV−vis DRS, and FT-IR/ATR. In addition, the activity of the Cr-MSU-*x*28 was compared with that of a reference catalyst prepared by incipient wetness impregnation but containing the same amount of chromium (Figure 15). The Cr-MSU-*x*28 catalyst shows about a 10% higher propylene yield, which demonstrates the superiority of the prepared Cr-MSU-*x* catalysts.

The TPR profile for the CrOx/MSU-*x* catalyst is shown in Supporting Information Figure S6. In agreement with the

dx.doi.org/10.1021/cs300198u | ACS Catal. 2012, 2, 1893−1903

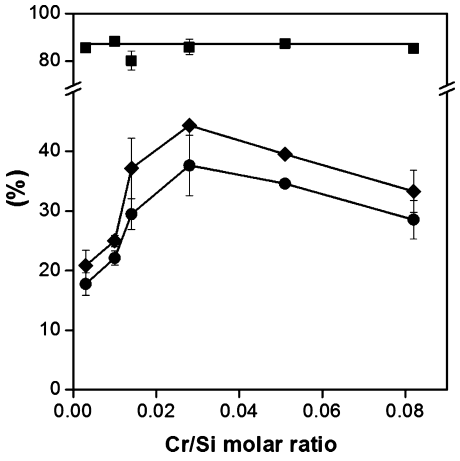

Figure 14. Variation in propane conversion, selectivity, and propylene yield over Cr-MSU-*x*N catalysts: (♦) propane conversion, (▲) propylene selectivity, and (●) propylene yield.

previous H_2-TPR results (Figure 8), CrO_x/MSU-*x* catalyst shows three distinct reduction peaks, which can be attributed to soft Cr(VI) and hard Cr(VI) as well as α-Cr_2O_3. Although the composition of soft Cr(VI) in total Cr(VI) appears to be high, the negative effect arising from α-Cr_2O_3, which is difficult to reduce, is more dominant, as evidenced by ODHP catalytic activity.

Determining the active site in chromium oxide has been a research goal for many years.[50] It has been revealed that the active site of chromium oxide in dehydrogenation reactions is a coordinatively unsaturated Cr(III) ion, as evidenced by in situ UV–vis DRS/ESR,[51,52] UV–vis DRS/Raman,[53,54] and FT-IR findings.[55] More specifically, Cr(III) ions can be classified into three types: Cr(III) ions formed by reduction of Cr(VI), dispersed Cr(III) ions as isolated center, and small Cr(III) clusters.[50] Among those classified Cr(III) ions, it appears that Cr(III) ions formed by reduction of Cr(VI) play a major role as an active site, in agreement with other investigators' results.[28,56] However, these investigators did not mention any classified prereduced Cr(VI) species, that is, isolated Cr(VI) and polymeric Cr(VI), since it has been almost impossible to discriminate between the individual contribution of these two types of Cr(VI) species to the overall catalytic activity.[31]

The TPR characterization results, in combination with the catalytic activity data, allow a detailed discussion of the nature of the active Cr(VI) species in the oxidative dehydrogenation of propane. The correlation between catalytic activity and the ratio of soft/total Cr(VI) is plotted in Figure 16a as a function of the Cr/Si molar ratio. Interestingly, they show similar trends, confirming the importance of the ratio between soft and total Cr(VI). For clarity of presentation, this relationship is presented in Figure 16b. On the basis of this graph, the composition of the soft Cr(VI) in the Cr-MSU-*x* catalysts appears to be a key factor for achieving a high performance in the oxidative dehydrogenation of propane. The correlation between the ratio of hard/total Cr(VI) area and the ODHP reaction activity of Cr-MSU-*x*N catalysts is presented in Figure 16c. As seen in the figure, the composition of hard Cr(VI) in total Cr(VI) has a negative effect on the ODHP catalytic activity.

Shishido et al.[49] proposed the dehydrogenation of propane reaction mechanism in the absence and presence of CO_2. In the case of ODHP reaction, oxidative dehydrogenation of propane proceeds through the reduction of Cr(VI) to Cr(III) in the initial stage of the reaction. After the initial stage of the reaction, the formed Cr(III) can also take part in direct dehydrogenation of propane. A part of Cr(III) can be oxidized to Cr(VI), and the reaction cycle can be formed. Assuming that propylene is produced simultaneously over Cr(VI) and Cr(III), three factors could have affected high performance in the oxidative dehydrogenation of propane: (i) in the initial stage of the reaction, soft Cr(VI), which is more easily reducible to Cr(III) than hard Cr(VI), leads to a higher yield of propylene through the oxidative dehydrogenation of propane; (ii) because the multinuclear Cr(III) originating from soft Cr(VI) exhibits higher turnover frequency than isolated Cr(III) site,[57] the dehydrogenation of propane on multinuclear Cr(III) would proceed more effectively; and (iii) Cr(III) originating from soft Cr(VI) can be more easily oxidized to Cr(VI) and take part in the reaction cycle again. On the basis of these results, we conclude that the composition of soft Cr(VI) in the Cr-MSU-*x* catalysts would be an important factor in the oxidative dehydrogenation of propane due to the effective participation of soft Cr(VI) in the redox cycle.

4. CONCLUSIONS

This study reports on a method for the synthesis of highly dispersed chromium oxide catalysts supported on MSU-*x* (Cr-MSU-*x*) and demonstrates the high catalytic activity of these materials for the oxidative dehydrogenation of propane using CO_2. These synthesized Cr-MSU-*x* catalysts showed superior

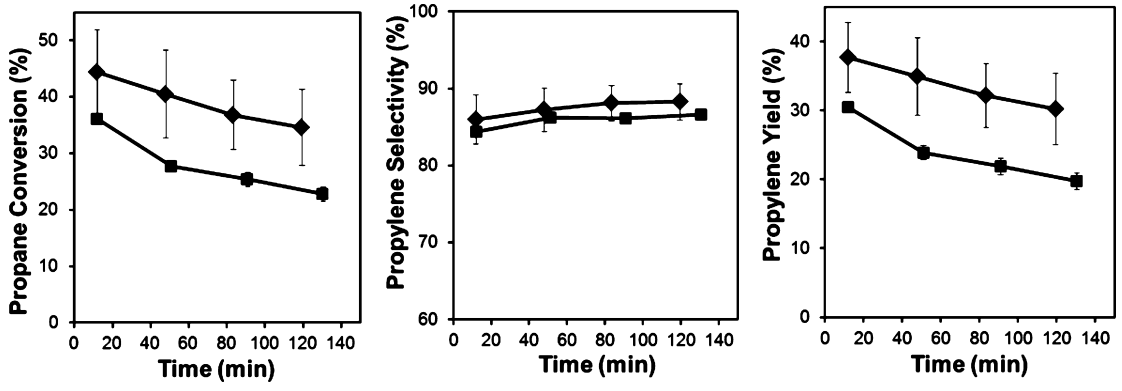

Figure 15. Comparison of propane conversion, selectivity, and propylene yield over the Cr-MSU-*x*N and CrO_x/MSU-*x* catalysts: (♦) Cr-MSU-*x*28 and (■) CrO_x/MSU-*x*.

dx.doi.org/10.1021/cs300198u | *ACS Catal.* 2012, 2, 1893–1903

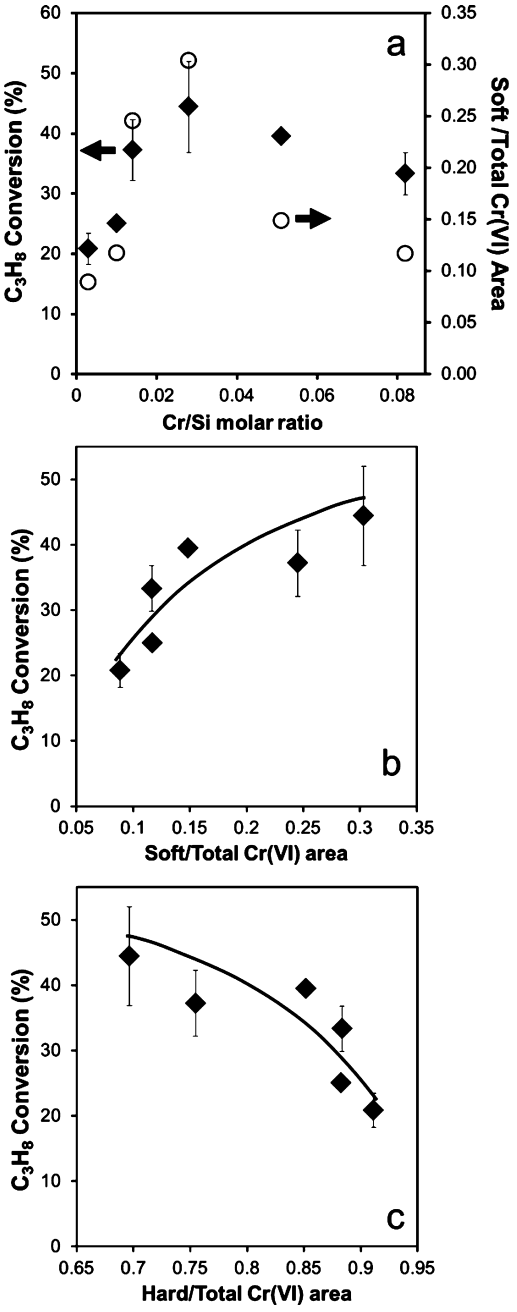

Figure 16. (a) Relationship between the ratio of soft/total Cr(VI) area and the initial ODHP reaction activity with respect to the Cr/Si molar ratio in Cr-MSU-*x*N catalysts. (b) Correlation between the ratio of soft/total Cr(VI) area and the initial ODHP reaction activity of Cr-MSU-*x*N catalysts. (c) Correlation between the ratio of hard/total Cr(VI) area and initial ODHP reaction activity of Cr-MSU-*x*N catalysts.

catalytic activity compared with a CrO_x/MSU-*x* catalyst prepared by conventional incipient wetness impregnation, which can be attributed to the fact that the chromium oxide is more highly dispersed on the MSU-*x* support in Cr-MSU-*x* catalysts. As the amount of chromium increased, the Cr-MSU-*x* catalysts contained various chromium species (isolated, dimers, polymeric species, and crystalline α-Cr_2O_3), which can be attributed to a polymerization phenomenon. In the H_2-TPR characterization, we were able to classify Cr(VI) into isolated Cr(VI) and polymeric Cr(VI) species, which were designated as hard Cr(VI) and soft Cr(VI), respectively. Moreover, the initial composition of soft Cr(VI) in Cr-MSU-*x* catalysts mainly affected ODHP catalytic activity. This suggests that coordinatively unsaturated Cr(III) formed during the reduction of soft Cr(VI) is more active than the reduced form of hard Cr(VI). The high activity of coordinatively unsaturated Cr(III) that originated from soft Cr(VI) can be rationalized by the fact that this type of chromium species promotes the reverse RWGS reaction and undergoes a more effective redox process during the ODHP reaction, as well.

■ ASSOCIATED CONTENT

Ⓢ Supporting Information

Additional information as noted in text. This information is available free of charge via the Internet at http://pubs.acs.org/

■ AUTHOR INFORMATION

Corresponding Author

*E-mail: jyi@snu.ac.kr.

Notes

The authors declare no competing financial interest.

■ ACKNOWLEDGMENTS

This work was financially supported by a grant from the GS Caltex Corporation. This research was also supported by the WCU (World Class University) program through the National Research Foundation of Korea funded by the Ministry of Education, Science and Technology (R31-10013).

■ REFERENCES

(1) Ren, Y.; Zhang, F.; Hua, W.; Yue, Y.; Gao, Z. *Catal. Today* **2009**, *148*, 316−322.
(2) Chen, M.; Xu, J.; Liu, Y. M.; Cao, Y.; He, H. Y.; Zhuang, J. H. *Appl. Catal., A* **2010**, *377*, 35−41.
(3) Liu, L.; Li, H.; Zhang, Y. *Catal. Commun.* **2007**, *8*, 565−570.
(4) Schimmoeller, B.; Jiang, Y.; Pratsinis, S. E.; Baiker, A. *J. Catal.* **2010**, *274*, 64−75.
(5) Michorczyk, P.; Ogonowski, J. *React. Kinet. Catal. Lett.* **2003**, *78*, 41−47.
(6) Salmanca, M.; Licea, Y. E.; Echavarria, A.; Faro, A. C., Jr.; Palacio, L. A. *Phys. Chem. Chem. Phys.* **2009**, *11*, 9583−9591.
(7) Liu, Y. M.; Cao, Y.; Yan, S. R.; Dai, W. L.; Fan, K. N. *Catal. Lett.* **2003**, *88*, 61−67.
(8) González, J. S.; Robles, J. M.; Rodríguez, M. A.; Torres, P. M.; Castellón, E. R.; López, A. J. *Catal. Lett.* **2000**, *64*, 209−214.
(9) Cavani, F.; Trifiro, R. *Catal. Today* **1995**, *24*, 307−313.
(10) Kotanjac, Ž. S.; Annaland, M. V. S.; Kuipers, J. A. M. *Chem. Eng. Sci.* **2010**, *65*, 441−445.
(11) Davies, T.; Taylor, S. H. *Catal. Lett.* **2004**, *93*, 151−154.
(12) Takehira, K.; Ohishi, Y.; Shishido, T.; Kawabata, T.; Takaki, K.; Zhang, Q.; Wang, Y. *J. Catal.* **2004**, *224*, 404−416.
(13) Sakurai, Y.; Suzaki, T.; Ikenaga, N.; Suzuki, T. *Appl. Catal., A* **2000**, *192*, 281−288.
(14) Li, H. Y.; Yue, Y.; Miao, C.; Xie, Z.; Hua, W.; Gao, Z. *Catal. Commun.* **2007**, *8*, 1317−1322.
(15) Wang, S.; Zhu, Z. H. *Energy Fuels* **2004**, *18*, 1126−1139.
(16) Chang, J. S.; Vislovskiy, V. P.; Park, M. S.; Hong, D. Y.; Yoo, J. S.; Park, S. E. *Green Chem.* **2003**, *5*, 587−590.
(17) Wang, S.; Murata, K.; Hayakawa, T.; Hamakawa, S.; Suzuki, K. *Appl. Catal., A* **2000**, *196*, 1−8.
(18) Michorczyk, P.; Ogonowski, J. *Appl. Catal., A* **2003**, *251*, 425−433.
(19) Daniell, W.; Ponchel, A.; Kuba, S.; Anderle, F.; Weingand, T.; Gregory, D. H.; Knözinger, H. *Top. Catal.* **2002**, *20*, 65−74.
(20) Kondratenko, E. V.; Brückner, A. *J. Catal.* **2010**, *274*, 111−116.

(21) Takahara, I.; Chang, W. C.; Mimura, N.; Saito, M. *Catal. Today* **1998**, *45*, 55−59.
(22) Rombi, E.; Cutrufello, M. G.; Solinas, V.; Rossi, S. D.; Ferraris, G.; Pistone, A. *Appl. Catal., A* **2003**, *251*, 255−266.
(23) Cherian, M.; Rao, M. S.; Hirt, A. M.; Wachs, I. E.; Deo, G. *J. Catal.* **2002**, *211*, 482−495.
(24) Liu, L. C.; Li, H. Q.; Zhang, Y. *Kinet. Catal.* **2009**, *50*, 684−690.
(25) Rao, T. V. M; Zahidi, E. M.; Sayari, A. *J. Mol. Catal. A: Chem.* **2009**, *301*, 159−165.
(26) Airaksinen, S. M. K.; Krause, A. O. I.; Sainio, J.; Lahtinen, J.; Chao, K. J.; Pérez, M. O. G.; Bañares, M. A. *Phys. Chem. Chem. Phys.* **2003**, *5*, 4371−4377.
(27) Hakuli, A.; Kytökivi, A.; Krause, A. O. I.; Suntola, T. *Appl. Catal., A* **2000**, *190*, 219−232.
(28) Liu, L.; Li, H.; Zhang, Y. *J. Phys. Chem. B* **2006**, *110*, 15478−15485.
(29) Hakuli, A.; Kytökivi, A.; I. Krause, A. O.; Suntola, T. *J. Catal.* **1996**, *161*, 393−400.
(30) Lezanska, M.; Szymanski, G. S.; Pietrzyk, P.; Sojka, Z.; Lercher, J. A. *J. Phys. Chem. C* **2007**, *111*, 1830−1839.
(31) Kumar, M. S.; Hammer, N.; Rønning, M.; Holmen, A.; Chen, D.; Walmsley, J. C.; Øye, G. *J. Catal.* **2009**, *261*, 116−128.
(32) Kim, S. S.; Pauly, T. R.; Pinnavaia, T. J. *Chem. Commun.* **2000**, 835−836.
(33) Zhao, X.; Wang, X. *J. Mol. Catal. A: Chem.* **2007**, 225−231.
(34) Zhang, L.; Zhao, Y.; Dai, H.; He, H.; Au, C. T. *Catal. Today* **2008**, *131*, 42−54.
(35) Wang, Y.; Ohishi, Y.; Shishido, T.; Zhang, Q.; Yang, W.; Guo, Q.; Wan, H.; Takehira, K. *J. Catal.* **2003**, *220*, 347−357.
(36) Weckhuysen, B. M.; Wachs, I. E.; Schoonheydt, R. A. *Chem. Rev.* **1996**, *96*, 3327−3349.
(37) Zhang, W.; Glomski, B.; Pauly, T. R.; Pinnavaia, T. J. *Chem. Commun.* **1999**, 1803−1804.
(38) Vuurman, M. A.; Hardcastle, F. D.; Wachs, I. E. *J. Mol. Catal.* **1993**, *84*, 193−205.
(39) Gaspar, A. B.; Brito, J. L. F.; Dieguez, L. C. *J. Mol. Catal. A: Chem.* **2003**, *203*, 251−266.
(40) Zhang, W.; Pinnavaia, T. J. *Catal. Lett.* **1996**, *38*, 261−265.
(41) Cavani, F.; Koutyrev, M.; Trifirò, F.; Bartolini, A.; Ghisletti, D.; Iezzi, R.; Santucci, A.; Piero, G. D. *J. Catal.* **1996**, *158*, 236−250.
(42) Michorczyk, P.; Ogonowski, J.; Kuśtrowski, P.; Chmielarz, L. *Appl. Catal., A* **2008**, *349*, 62−69.
(43) Li, C.; Stairs, P. C. *Stud. Surf. Sci. Catal.* **1996**, *101*, 881−890.
(44) McMillan, P.; Piriou, B. *J. Non-Cryst. Solids* **1982**, *53*, 279−298.
(45) Ivanova, T.; Gesheva, K.; Cziraki, A.; Szekeres, A.; Vlaikova, E. *J. Phys.: Conf. Ser.* **2008**, *113*, 012030.
(46) Hakuli, A.; Harlin, M. E.; Backman, L. B.; Krause, A. O. I. *J. Catal.* **1999**, *184*, 349−356.
(47) Liu, L.; Li, H.; Zhang, Y. *Catal. Today* **2006**, *115*, 235−241.
(48) Weckhuysen, B. M.; Wachs, I. E. *J. Phys. Chem.* **1996**, *100*, 14437−14442.
(49) Shishido, T.; Shimamura, K.; Teramura, K.; Tanaka, T. *Catal. Today* **2012**, *185*, 151−156.
(50) Weckhuysen, B. M.; Schoonheydt, R. A. *Catal. Today* **1999**, *51*, 223−232.
(51) Bruckner, A. *Chem. Commun.* **2001**, *20*, 2122−2123.
(52) Bruckner, A. *Phys. Chem. Chem. Phys.* **2003**, *5*, 4461−4472.
(53) Nijhuis, T. A.; Tinnemans, S. J.; Visser, T.; Weckhuysen, B. M. *Phys. Chem. Chem. Phys.* **2003**, *5*, 4361−4365.
(54) Nijhuis, T. A.; Tinnemans, S. J.; Visser, T.; Weckhuysen, B. M. *Chem. Eng. Sci.* **2004**, *59*, 5487−5492.
(55) Rossi, S. D.; Ferraris, G.; Fremiotti, S.; Garrone, E.; Ghiotti, G.; Campa, M. C.; Indovina, V. *J. Catal.* **1994**, *148*, 36−46.
(56) Weckhuysen, B. M.; Bensalem, A.; Schoonheydt, R. A. *J. Chem. Soc., Faraday Trans.* **1998**, *94*, 2011−2014.
(57) Puurunen, R. L.; Weckhuysen, B. M. *J. Catal.* **2002**, *210*, 418−430.